

# Exceptionally preserved 'skin' in an Early Cretaceous fish from Colombia

Andrés Alfonso-Rojas<sup>1,\*</sup> and Edwin-Alberto Cadena<sup>1,2,\*</sup>

<sup>1</sup>Facultad de Ciencias Naturales, Grupo de Investigación Paleontología Neotropical Tradicional y Molecular (PaleoNeo), Universidad del Rosario, Bogotá, Colombia

<sup>2</sup>Smithsonian Tropical Research Institute, Panama City, Panama

\*These authors contributed equally to this work.

## ABSTRACT

Studies of soft tissue, cells and original biomolecular constituents preserved in fossil vertebrates have increased greatly in recent years. Here we report preservation of 'skin' with chemical and molecular characterization from a three-dimensionally preserved caudal portion of an aspidorhynchid Cretaceous fish from the equatorial Barremian of Colombia, increasing the number of localities for which exceptional preservation is known. We applied several analytical techniques including SEM-EDS, FTIR and ToF-SIMS to characterize the micromorphology and molecular and elemental composition of this fossil. Here, we show that the fossilized 'skin' exhibits similarities with those from extant fish, including the wrinkles after suffering compression stress and flexibility, as well as architectural and tissue aspects of the two main layers (epidermis and dermis). This similarity extends also to the molecular level, with the demonstrated preservation of potential residues of original proteins not consistent with a bacterial source. Our results show a potential preservation mechanism where scales may have acted as an external barrier and together with an internal phosphate layer resulting from the degradation of the dermis itself creating an encapsulated environment for the integument.

**Subjects** Biochemistry, Paleontology, Zoology

**Keywords** Aspidorhynchidae, Barremian, Zapatoca, South America, Soft-tissue, Molecular Paleontology

Submitted 4 March 2020

Accepted 14 June 2020

Published 8 July 2020

Corresponding author  
Edwin-Alberto Cadena,  
edwin.cadena@urosario.edu.co

Academic editor  
Virginia Abdala

Additional Information and  
Declarations can be found on  
page 16

DOI 10.7717/peerj.9479

© Copyright  
2020 Alfonso-Rojas and Cadena

Distributed under  
Creative Commons CC-BY 4.0

## OPEN ACCESS

## INTRODUCTION

Exceptional preservation in the fossil record is expressed in a wide range of structures including hair, cells, blood vessels, claw sheaths, feathers, pycnofibers, muscle remains, skin and even the potential remains of original biomolecular constituents (DNA, proteins, lipids) (Lingham-Soliar & Plodowski, 2010; Cadena, 2016; Cadena & Schweitzer, 2012; Cleland et al., 2015; McNamara et al., 2018a; Schweitzer, 2011; Wiemann et al., 2018; Bailleul et al., 2020) associated with these structures. The skin is the largest organ of the a vertebrate body, which encloses or covers their entire body. Numerous integumentary derivatives are located within the epithelial sheet itself (glands) or extend above its surface (teeth, scales, feathers, hairs, etc.) (Chernova, 2009). The skin of vertebrates and its derivate structures has been shown to have high preservation potential in the fossil record, and has been reported in dinosaurs, pterosaurs, snakes, frogs and birds (McNamara et al.,

2018a; McNamara et al., 2016; McNamara et al., 2009; McNamara et al., 2018b; Varejão et al., 2019). Similarly, fishes are also covered by a relatively flexible skin, which in almost all extant and extinct groups is associated with hard scales composed of collagen I, calcium salts (Sionkowska & Kozłowska, 2014), ganoine and cosmine. Preservation of skin in fossil fish has been documented in many Konservat Lagerstätte sites, including the Messel Formation, Germany (Micklich, 2002), Huajiying and Yixian formations (Xu et al., 2020); and Romualdo Formation (previously Santana Formation) of northeastern Brazil (Kellner et al., 2013; Maisey, 1991; Martill, 1989; Fig. 1D).

Despite the abundant recent discoveries of fossil vertebrates from the Cretaceous of Colombia (Cadena, 2015; Cadena & Parham, 2015; Cadena et al., 2019; Carballido et al., 2015; Maxwell et al., 2019; Noé & Gómez-Pérez, 2020; Páramo-Fonseca et al., 2016; Vernygora et al., 2018), the exceptional preservation of soft tissue or their potential original components is still rarely reported for most of them, with the exception of the recently described gravid marine turtle from the Early Cretaceous of Villa de Leyva (Cadena et al., 2019). Here we report a caudal fragment of an aspidorhynchid fossil fish recovered from the lower segment of the Paja Formation from Zapatoca, Santander, Colombia (Figs. 1A–1C) that constitutes the first specimen of the paleontological collection at Universidad del Rosario in Bogotá. We have applied multiple analytical techniques to interrogate the degree of preservation of its skin, including some of their potentially original biomolecular constituents. Our finding not only expands the worldwide record of skin preserved in Cretaceous vertebrates, but also constitutes the most equatorial example of it (Fig. 1D) considering that Colombia has barely changed its latitude since the Early Cretaceous (Fig. S1).

## MATERIALS & METHODS

**Fossil material Collection and Geological framework.** UR-CP-0001 specimen was collected by E-A. Cadena in 2016, during a short expedition to Zapatoca. The fossil was found approximately 100 m north-west from the Radio Lenguerke station antenna region, Zapalonga locality (6°48'28.94"N, 73°16'08.23"W, 1703 m) (Fig. 1A), inside a gray-purple sequence dominated by mudstones with abundant occurrence of large concretions and interbedded layers of fossiliferous limestones (Fig. 1B). This sequence represents the most basal member of the Paja Formation in this zone, a few meters above the last limestone bank of the underlying Rosablanca Formation. Approximately 35 m of stratigraphic column were measured and described (Fig. 1C).

The fossil was collected using sterile nitrile gloves and wrapped in aluminum foil, and placed in a plastic bag with silica gel small packets to control humidity. To avoid any contamination, the fossil has not been treated mechanically or chemically and always has been manipulated using sterile nitrile gloves for measurements, photography or sampling for analytical studies. Fieldwork and laboratory experiments permit granted by the Comité de ética and the Dirección de Investigaciones of the Universidad del Rosario (IV-FCS018).

**Specimen photography, internal observation and measurements.** General views of UR-CP-0001 specimen were obtained using a Leica-EZ4-HD and Nikon SMZ1270

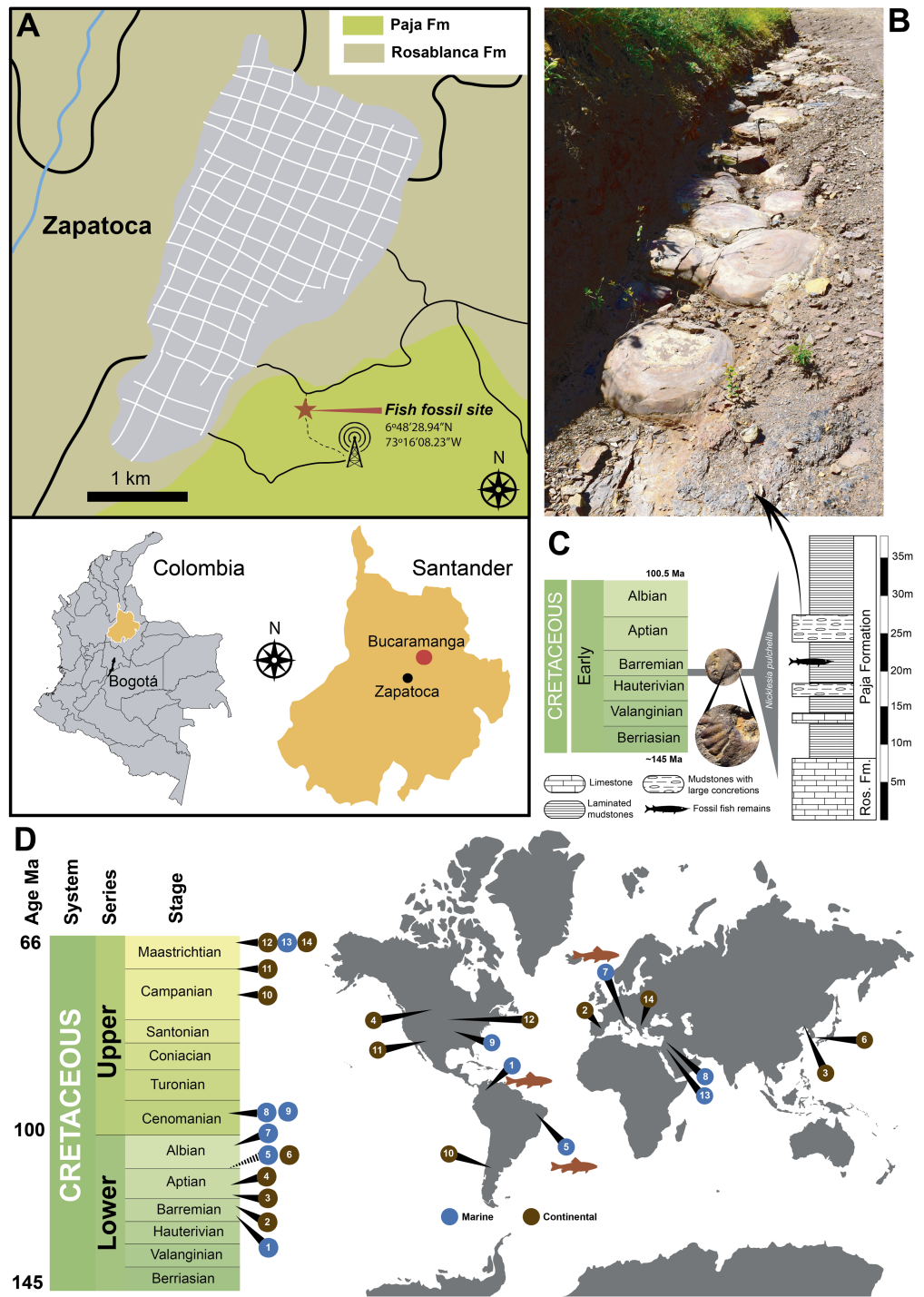


**Figure 1** Locality and other reported exceptionally preserved skin fossils from the Cretaceous. (A) map of Colombia showing in orange the Santander department, and the fish fossil site (Zapalunga locality) very near Zapatoaca. (B) outcrop view at the fish fossil site, showing the presence of mudstones and large concretions. (C) stratigraphic column along with Zapalunga locality, indicating the (continued on next page...)

Full-size DOI: 10.7717/peerj.9479/fig-1

**Figure 1 (...continued)**

horizon where UR-CP-0001 was found. (D) world map with remarkable findings of exceptional preserved skin fossils through the Cretaceous: (1) Barremian, Paja Fm, Colombia (this study); (2) Barremian, Calizas de la Huérgina Fm, Spain ([Martin et al., 2015](#)); (3) Barremian-Aptian, Huajjiying and Yixian formations ([Xu et al., 2020](#)) Yixian Fm, China ([Lingham-Soliar & Plodowski, 2010](#)); (4) Aptian, Clearwater Fm, Canada ([Brown et al., 2017](#)); (5) Aptian-Albian, Romulado Fm, Brazil ([Martill, 1988](#)); (6) Aptian-Albian, Haman Fm, South Korea ([Paik, Kim & Huh, 2010](#)); (7) Albian, Pietraraja, Italy ([Signore et al., 2005](#)); (8) Cenomanian, Hadjula, Lebanon ([Caldwell & Sasso, 2004](#)); (9) Cenomanian, Nobrara Fm, Kansas, United States ([Lindgren, Everhart & Caldwell, 2011a](#)); (10) Campanian, Auca Mahuevo, Argentina ([Coria & Chiappe, 2007](#)); (11) Campanian-Maastrichtian, Fruitland Fm, New Mexico, United States ([Hall, Wolberg & West, 1988](#)); (12) Maastrichtian, Hell Creek Fm, North Dakota, United States ([Manning et al., 2009](#)); (13) Maastrichtian Harrana, Jordan ([Lindgren, Kaddumi & Polcyn, 2013](#)); (14) Maastrichtian, Sânpetru Fm, Romania ([Grellet-Tinner et al., 2012](#)).

stereomicroscopes coupled with cameras. Measurements of the specimen were obtained using calipers, always wearing nitrile gloves during its manipulation. The specimen was scanned using computer tomography (CT-scan), Toshiba Aquilion at the Radiology unit of Hospital Méderi, Bogotá, with the following parameters: voltage 120 kV, exposure 225 mAs, and voxel size 350  $\mu\text{m}$ .

**Transmitted and polarized light microscopy.** In order to observe and obtain microscopic details of the preserved ‘skin’, small pieces of approximately five  $\text{mm}^3$  each were sampled and treated separated with HCl 25% for 24 h and EDTA 0.5 M pH 8.0 for 4 days changing daily to dissolve carbonate matrix and full demineralization. The isolated remains of ‘skin’ were rinsed 3 times with E-Pure water to remove HCl and EDTA, then were mounted in glass slides, observed and photographed using a Nikon ECLIPSE-80i transmitted-light microscope and an Olympus CX-31 polarized microscope. Samples were finally transferred to sterilized containers for Fourier-transform infrared spectroscopy (FTIR) analyses.

**FTIR spectroscopy.** Samples from an extant *Oreochromis* sp. (Mojarra fish), and four samples from the UR-CP-0001 fossil fish (‘skin’ from HCl, EDTA treatments, ‘skin’ untreated and infilling matrix) were analyzed. The FTIR spectra were collected in the mid-infrared range of 4,000–600  $\text{cm}^{-1}$  wavelength using a Bruker Optics - ALPHA ZnSe FTIR spectrometer at the Biomedical Engineering Lab of Universidad de los Andes, Bogotá, Colombia. Between each analysis, the crystal and sample holder of the spectrometer were cleaned up with isopropanol and standardized with an “air” measurement in order to reduce rovibration absorptions of carbon dioxide present in the ambient air. Measurements were repeated twice for each of the samples. For the ‘skin’ untreated spectrum a deconvolution was performed for the 1,450–1,800  $\text{cm}^{-1}$  range in order to find out the specific peaks associated to the vibrational band frequencies of Amide I and II, similar as described in [Kong & Yu \(2007\)](#).

**Scanning electron microscopy and elemental analysis (SEM-EDS).** Four different regions of the fossil fish were sampled for Scanning Electron Microscope (SEM)-coupled with Energy Dispersive X-ray Spectroscopy (EDS) observation and characterization, taking  $\sim 5 \text{ mm}^3$  of each (scale ‘skin’, and two different regions of the infilling matrix exhibiting different coloration). Samples were mounted in sterile carbon stubs and storage in sterile boxes prior to the SEM-EDS analyses, which were performed at the Microscopy Core Facility of Universidad de los Andes, Bogotá, Colombia. Samples were analyzed without

adding any coating. Imaging and map elemental composition were obtained at 10 kV using a JEOL-JSM-6490 LV SEM, while the point elemental composition was performed at 10 kV using a TESCAN-Lyra3 SEM.

**Time of Flight Secondary Ions Mass Spectrometry (ToF-SIMS).** Two samples from the UR-CP-0001, an untreated (fresh) and an HCl treated were mounted in sterilized glass and sent to the Analytical Instrumentation Facility (AIF) of North Carolina State University, Raleigh, North Carolina. ToF-SIMS analyses were conducted using a TOF SIMS V (ION TOF, Inc. Chestnut Ridge, NY) instrument equipped with a  $\text{Bi}_n^{m+}$  ( $n = 1-5$ ,  $m = 1, 2$ ) liquid metal ion gun,  $\text{Cs}^+$  sputtering gun and electron flood gun for charge compensation. Both the Bi and Cs ion columns are oriented at  $45^\circ$  with respect to the sample surface normal, with at least two different regions of the sample being analyzed. The instrument vacuum system consists of a load lock for rapid sample loading and an analysis chamber, separated by the gate valve. The analysis chamber pressure is maintained below  $5.0 \times 10^{-9}$  mbar to avoid contamination of the surfaces to be analyzed.

For high mass resolution spectra acquired in this study, a pulsed  $\text{Bi}_3^+$  primary ion beam at 25 keV impact energy with less than 1 ns pulse width was used. An electron gun was used to prevent charge buildup on the insulating sample surfaces. The total accumulated primary ion dose for data acquisition was less than  $1 \times 10^{13}$  ions/cm<sup>2</sup>, an amount of ions which is within the static SIMS regime. The mass resolution on Si wafer is about  $\sim 8,000$  m/ $\Delta m$  at 29AMU. For high lateral resolution mass spectral images acquired in this study, a Burst Alignment setting of 25 keV  $\text{Bi}_3^+$  ion beam was used to raster a 500  $\mu\text{m}$  by 500  $\mu\text{m}$  area. The negative secondary ion mass spectra obtained were calibrated using  $\text{C}^-$ ,  $\text{O}^-$ ,  $\text{OH}^-$ ,  $\text{C}_n^-$ , respectively. The positive secondary ion mass spectra were calibrated using  $\text{H}^+$ ,  $\text{C}^+$ ,  $\text{C}_2\text{H}_3^+$ ,  $\text{C}_3\text{H}_5^+$ ,  $\text{C}_4\text{H}_7^+$ .

## RESULTS

### Systematic Paleontology

Order ASPIDORHYNCHIFORMES Bleeker, 1859

Family ASPIDORHYNCHIDAE Nicholson and Lydekker, 1889

Genus and Species Indet. (Fig. 2)

Referred material.—UR-CP-0001, caudal portion of a fish, missing the fins.

Locality and Age.—Radio Lenguerke station antenna region, Zapalonga locality ( $6^\circ 48' 28.94''\text{N}$ ,  $73^\circ 16' 08.23''\text{W}$ , 1,703 m), southeast of Zapatoca, Santander Department, Colombia. The occurrence of the ammonoid *Nicklesia pulchella* (Fig. 1C) found in the same layer and concretions cropping out at this locality, indicates an early Barremian age for this locality following (Patarroyo, 2009; Patarroyo, 2020).

Remarks.—UR-CP-0001 is attributed to the Aspidorhynchidae family by the presence of rectangular high hypertrophied flank and nearly subquadrate scales covering the lateral and ventral sides of the trunk (Brito, 1997; Cantalice, Alvarado-Ortega & Brito, 2018) (Figs. 2G–2J). Although further taxonomic resolution is not possible owing to its

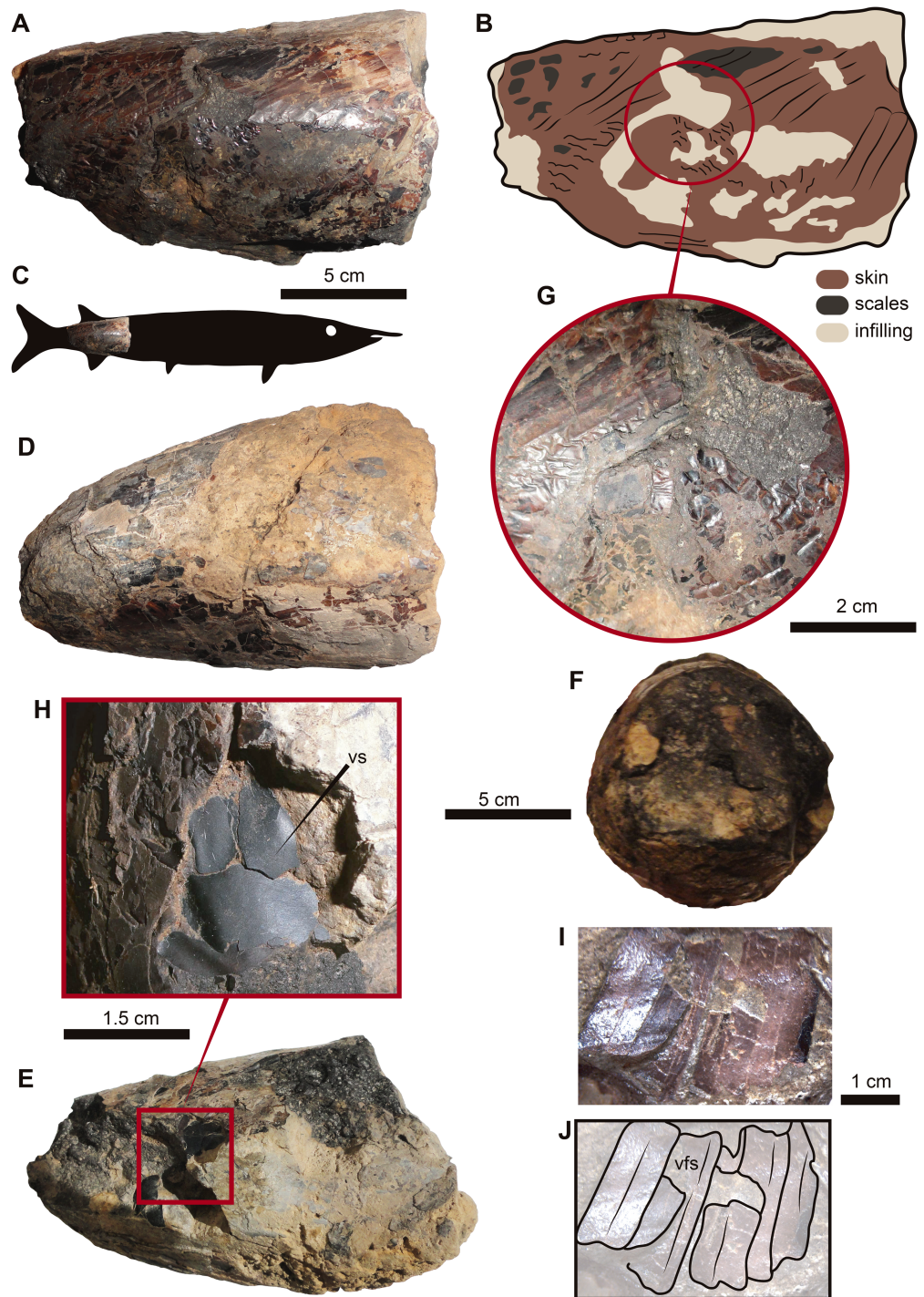


**Figure 2** UR-CP-0001, aspidorhynchid fossil fish specimen. (A–B) right lateral view. (C) interpreted position of UR-CP-0001 in the body of an aspidorhynchid fish. (D) left lateral view. (E) ventral view. (F) posterior view, showing the naturally preserved original 3-D volume. (G) detail of the originally preserved ‘skin’ with wrinkles and marks. (H) View of some of the ventral scales (vs) preserved. (I–J) elongated ventral flank scales (vfs). five cm scale applies for A, D, E and F; two cm for G; 1.5 cm for H and one cm for I and J.

Full-size DOI: [10.7717/peerj.9479/fig-2](https://doi.org/10.7717/peerj.9479/fig-2)

fragmentary preservation, the smooth surface of the flank scales resemble those of *Vinctifer comptoni* (see [Cantalice, Alvarado-Ortega & Brito, 2018](#)), suggesting the possibility that this organism represents a member of this taxon. Aspidorhynchids constitute an extinct basal teleostean group from the Middle Jurassic to Late Cretaceous fishes that were highly specialized and lived in shallow epicontinental marine environments throughout America, Europe, Australia, Africa, Antarctica, and Middle East ([Cantalice, Alvarado-Ortega & Brito, 2018](#)). The occurrence of the aspidorhynchid *Vinctifer* has been previously reported from exposures of the Paja Formation cropping out near Villa de Leyva, in the Department of Boyacá ([Noé & Gómez-Pérez, 2020](#); [Schultze & Stöhr, 1996](#)).

**Description.** UR-CP-0001 represents a caudal portion of a fish preserved three-dimensionally ([Figs. 2A–2D](#)). The specimen is shaped like a truncated cone, which fits with the shape of caudal portions of other aspidorhynchids previously reported ([Fig. 2C](#)). Also the orientation of the scales impressions left on the skin exhibits a pattern typical of the caudal region ([Fig. 2B](#)).

The fossil has a length of 128.5 mm, an anterior height of 84 mm, and a posterior height of 40 mm. On the ventral surface there is a region that shows a scar that resembles the potential insertion of the anal fin. The edges of the specimen are completely eroded and no sign of bones is visible, which suggests that most of the anterior part of the specimen was probably lost prior the fossilization

Most of the lateral surfaces of the specimen bear a brown, wrinkled layer preserving ‘skin’ and covered in some places by rectangular black scales ([Fig. 2B](#)). These are particularly visible on the right side ([Fig. 2G](#)), whereas on the ventral side there are small, square marks similar to the ventral scales ([Figs. 2H, 2I](#)). There are no vertebrae or spines visible on the naturally broken anterior or posterior surfaces ([Figs. 2E, 2F](#)) nor are any visible internally in Computed Tomography (CT) of the specimen, which is infilled by a heterogeneous black-gray and yellow carbonate matrix (hereinafter infilling matrix) that is high-porosity in some regions and reacts to HCl ([Video S1](#)).

After demineralization with either HCl or EDTA ([Figs. 3A, 3B](#)) isolated pieces of ‘skin’ from fragments of fossil material (handled following aseptic techniques (see methods) and no glues or preservatives were applied) were observed under transmitted light microscope, and were shown to be formed by two distinct layers. Similar layers were observed in the dry skin of the extant *Oreochromis* sp. (Mojarra fish) ([Fig. 3C](#)) together to some parallel lines similar to fibers observed in the extant and the fossil ([Figs. 3D, 3F, 3G](#)). The most basal layer is a thin semitransparent film-like sheet; this layer is covered by a brown to black organic patchy layer, in some degraded regions form irregular reticular pattern ([Figs. 3I–3K](#)). The basal semitransparent layer is quite flexible when wet, but becomes rigid and fragile when dried ([Video S2](#)). Under polarized light, the basal layer of the HCl-treated samples exhibits small granules having a first order of birefringence, indicating a potential phosphatic composition. The external organic brown layer covering this basal layer remains of the same color when the polarizer is rotated ([Figs. 3L–3M](#)). Pieces treated with EDTA showed higher degradation characterized by less and smaller fragments of both layers in contrast to those treated with HCl ([Fig. S1](#)). We consider that the external organic brown layer is consistent with the most exterior morphological feature of the skin, which is the

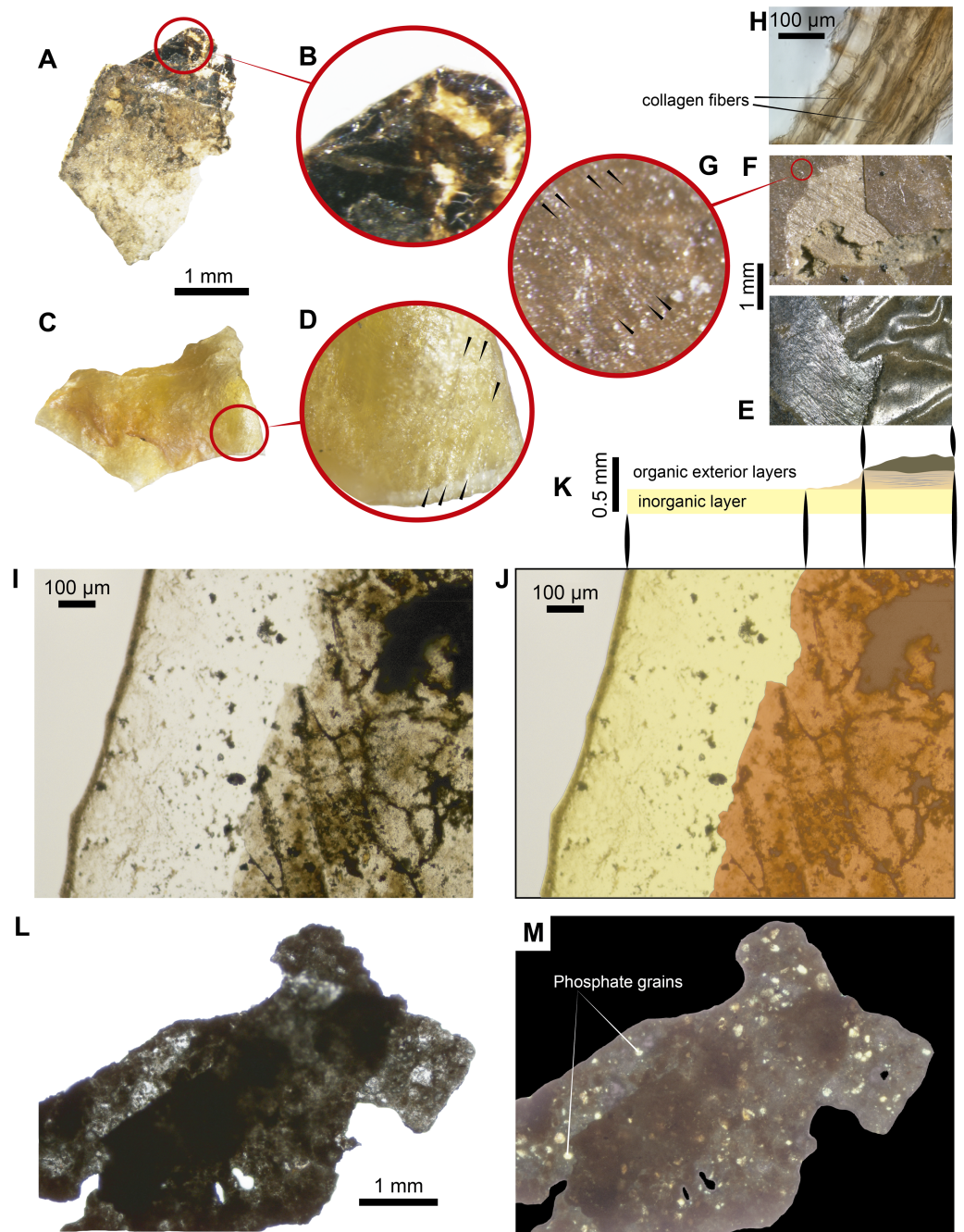


**Figure 3** Some 'skin' fragments after HCl treatment. (A) Light micrograph of preserved 'skin' after treated with 15% HCl, without any infilling matrix left. (B) Enlargement of the organic patchy layer. (C–D) Fragment of the dry skin of the extant *Oreochromis* sp. (Mojarra fish) exhibiting two layers, wrinkles and collagen fibers indicated by black arrows in d. (E) Wrinkled 'skin' of UR-CP-0001. (F–G) An UR-CP-0001 close-up of the two organic exterior layers and collagen fibers indicated by black arrows in g. (H) isolated tissue fragment after EDTA treatment under transmitted-light microscopy showing collagen fibers. (I–K) An UR-CP-0001 'skin' fragment under transmitted-light microscope, exhibiting the two distinct inorganic (base) and organic (exterior) layers. (L–M) An UR-CP-0001 'skin' fragment under transmitted-light (L) and polarized-light (M), showing low birefringence of the granular basal layer. One mm horizontal scale applies for A, C, L and M; one mm vertical scale for E and F.

Full-size [DOI: 10.7717/peerj.9479/fig-3](https://doi.org/10.7717/peerj.9479/fig-3)



epidermis (Elliott, 2011); also soft-tissue that are morphologically consistent with portions of the dermis were recovered after EDTA treatment, exhibiting collagen fibers (Fig. 3H).

**SEM-EDS results.** The untreated, uncoated skin is very smooth and uniform under SEM, which contrasts with the highly granular topography of the surrounding infilling matrix (Figs. 4A–4D). Point elemental analyses show predominant occurrence of carbon and nitrogen, with minor representation of calcium and phosphorus in the ‘skin’ layer (Fig. 4C). The infilling matrix contains predominantly calcium and carbon; no nitrogen was observed (Fig. 4D). Similar results were obtained using elemental mapping of the ‘skin’ and matrix (Figs. 4G–4L); however, nitrogen was not clearly observed.

**FTIR results.** The FTIR spectrum of the untreated ‘skin’ sample showed distinct peaks at  $2,931\text{ cm}^{-1}$ ,  $1,740\text{ cm}^{-1}$ ,  $1,591\text{ cm}^{-1}$  and around  $1,120\text{ cm}^{-1}$ . The EDTA-treated sample showed high infrared absorption peaks at  $1,703$ ,  $1,540$  and  $3,744\text{ cm}^{-1}$  respectively (Fig. 5A). The HCl-treated sample showed absorption peaks at  $1,724$ ,  $1,142$ , and  $1,027\text{ cm}^{-1}$  (Fig. 5A). The commercial extant fish skin sample (*Oreochromis* sp. mojarra fish), exhibited two well defined regions of peaks at  $1,746$ ,  $1,647$ ,  $1,559$ , and  $1,117\text{ cm}^{-1}$  and second one with peaks at  $3,319$  and  $2,931\text{ cm}^{-1}$ . In contrast, the infilling matrix from UR-CP-0001 showed clear peaks at  $1,428\text{ cm}^{-1}$ ,  $1,030\text{ cm}^{-1}$ ,  $876\text{ cm}^{-1}$  and  $711\text{ cm}^{-1}$  (Fig. 5A).

**ToF-SIMS results.** ToF-SIMS analyses of both the untreated fossil ‘skin’ and the HCl-treated ‘skin’ show almost the same as each other negative and positive ions spectra (Fig. 6, Fig. S2); in particular, in abundance of  $\text{CN}^-$  (Fig. 6C) and  $\text{CNO}^-$  (Fig. 6F) negative ions;  $\text{CH}_4\text{N}^+$  (Fig. 6D),  $\text{C}_4\text{H}_8\text{N}^+$  (Fig. 6E),  $\text{C}_2\text{H}_6\text{N}^+$  (Fig. 6G), and  $\text{C}_3\text{H}_6\text{N}^+$  (Fig. 6H) positive ions were detected. All ions potentially derived from proteins are presented in Table 1, as well as all raw data obtained from ToF-SIMS analyses can be found in Data S1.

**Integrated compositional characterization of the ‘skin’ and comparisons.** As we showed using transmitted light, polarized light, and SEM-EDS microscopy (Figs. 3 and 4), the preservation of the ‘skin’ in UR-CP-0001 resulted from an organic and inorganic interaction forming two well defined layers (Figs. 3J, 3K), each of them exhibiting distinct physical and chemical characteristics. The basal layer is translucent, granular to film-like in appearance. This layer is interpreted as inorganic in composition, potentially phosphates, based on its birefringence pattern (Fig. 3M), the abundance of phosphorus showed by the EDS analysis (Fig. 4G, K-Phosphorus) together with the high absorbance peaks at  $1,177$  and  $998\text{ cm}^{-1}$  observed in the FTIR spectra. These peaks are particularly intense in the UR-CP-0001 sample (Fig. 5A), and were reported in an FTIR analysis of *Vinctifer comptoni* from the Cretaceous of Brazil (Sousa Filho et al., 2016). Similar peaks at this region have been interpreted as four infrared absorption bands of phosphate ( $\nu\text{PO}_4^{3-}$   $1,120\text{ cm}^{-1}$ ,  $\nu_{3a}\text{ PO}_4^{3-}$   $1,112\text{ cm}^{-1}$ ,  $\nu_{3c}\text{ PO}_4^{3-}$   $1,007\text{ cm}^{-1}$  and  $\nu_1\text{ PO}_4^{3-}$   $966\text{ cm}^{-1}$ ) (Lee et al., 2017). Occurrence of phosphates and carbonates could be inferred from both SEM-EDS and FTIR analyses (Figs. 4K, 4L ; 5A) in the infilling matrix similar to the typical calcium carbonate FTIR spectrum (Bosch-Reig, Gimeno-Adelantado & Moya-Moreno, 2002). The more external layer of the ‘skin’ in UR-CP-0001 is brown to black, and is consistent with organic material when analyzed under polarized light (Fig. 3M). Its organic composition is supported by the SEM-EDS point and map analyses, which showed particularly high levels of carbon and nitrogen (Figs. 4C, 4H). Another remarkable finding that supports

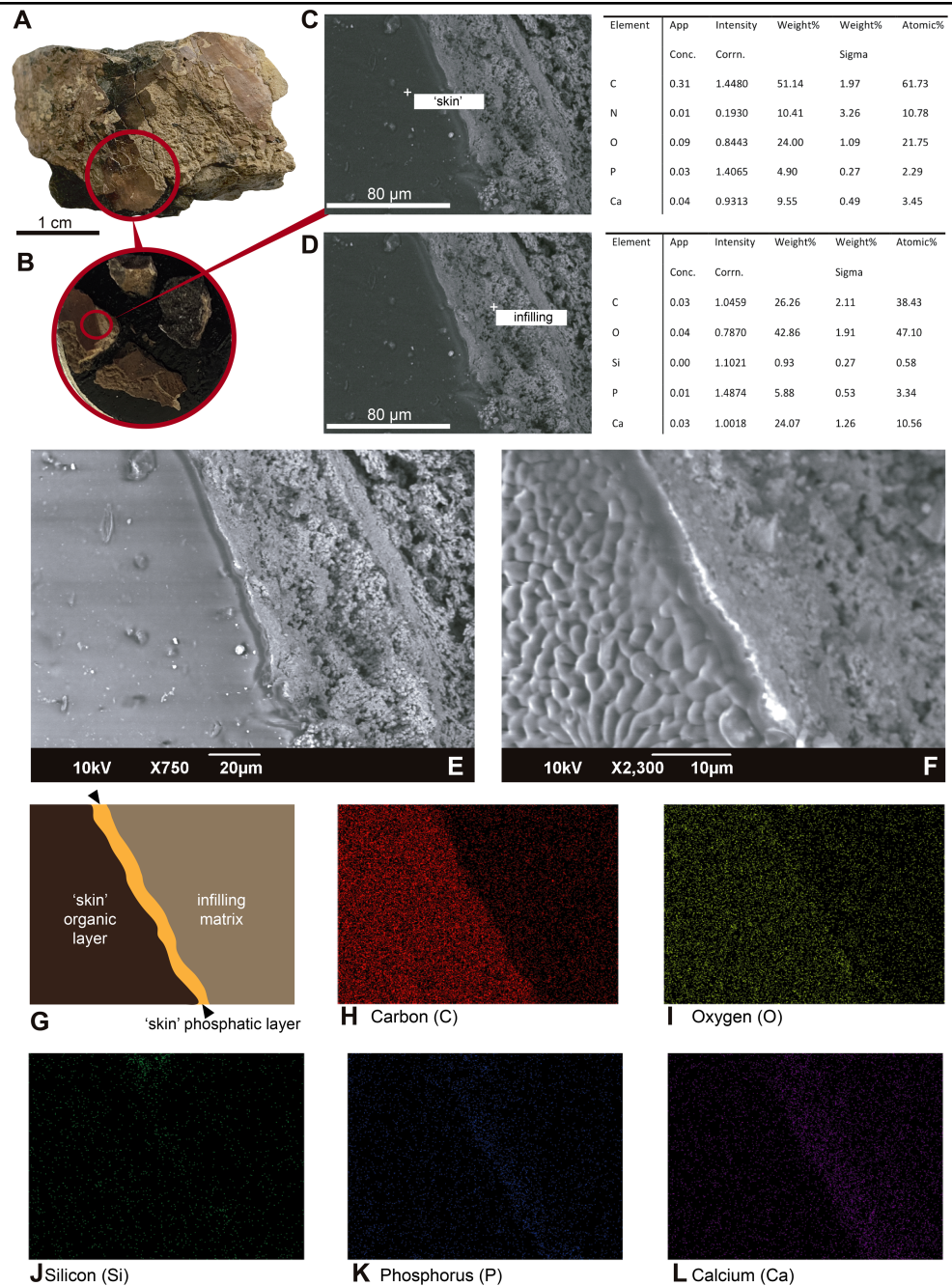


**Figure 4** SEM-EDS micrographs and elemental composition analyses of an untreated and uncoated fragment of UR-CP-0001 'skin'. (A) Sample from UR-CP-0001 that contains 'skin' and infilling matrix. (B) detail of samples mounted over the stub. (C) SEM micrograph with point EDS analysis in the 'skin' region, showing the abundant content of carbon and nitrogen, with less occurrence of calcium and phosphorus. (D) SEM micrograph with point EDS analysis in the infilling matrix, showing absence of nitrogen, dominance of carbon and calcium instead. (E) SEM micrograph of the 'skin'-infilling matrix contact before apply the EDS analysis. (F) Same micrograph as in (E) after EDS analysis, showing the extremely wrinkled organic surface of the 'skin', remaining intact the infilling matrix region. (G) Outline of the 'skin' organic and phosphatic layer, as well as the infilling matrix showed in e, which is the base of the elemental mapping. (H-L) Elemental mapping at 10 kV of the 'skin' infilling matrix region showing dominance of carbon (H) and oxygen (I) at the organic region, and phosphorus (K) at the boundary between the 'skin' and the infilling matrix; silicon (J) is very scarce in both regions, and of calcium (L) is highly abundant in the infilling-matrix.

Full-size DOI: [10.7717/peerj.9479/fig-4](https://doi.org/10.7717/peerj.9479/fig-4)

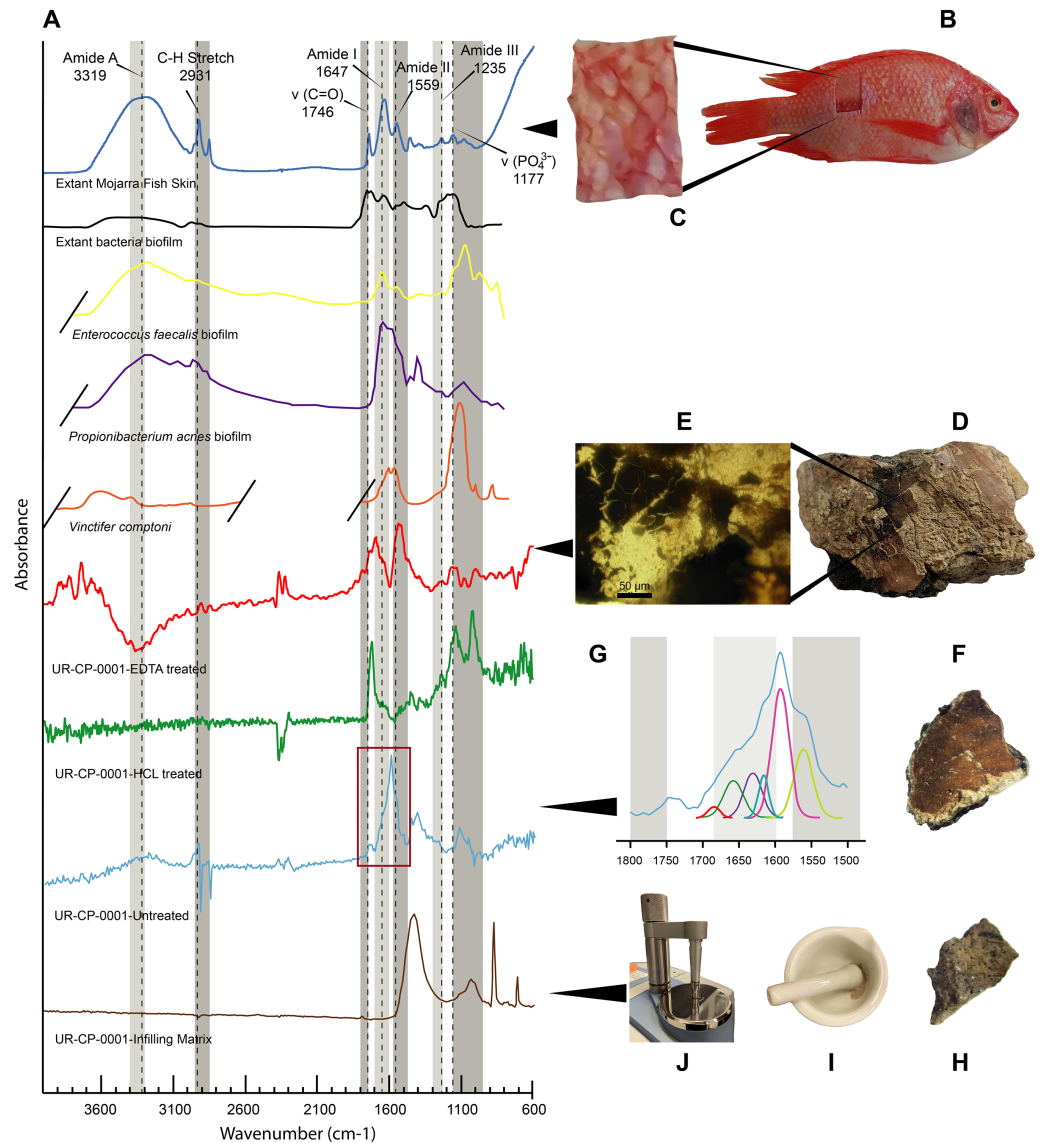


**Figure 5** FTIR analyses of UR-CP-0001 and the extant *Oreochromis* sp. (A) Composite FTIR spectra (absorbance vertical axis, wavenumber horizontal axis) of different samples: *Oreochromis* sp. (Mojarra fish) (dark blue line) with interpretation of typical proteinaceous compounds (Amide A, I, II, III,  $\nu(\text{C}=\text{O})$ , C-H stretch and a phosphate) with gray bands showing potential ranges based on [Boatman et al. \(2019\)](#); [Kong & Yu \(2007\)](#); and [Lee et al. \(2017\)](#); an extant bacteria biofilms (black, yellow and purple lines) taken and redraw from [Lee et al. \(2017\)](#) and [Lindgren et al. \(2011b\)](#); *Vinctifer comptoni* (orange line) from the Cretaceous of Brazil, taken and redrawn from [Sousa Filho et al. \(2016\)](#); UR-CP-0001 aspidorhynchid fossil fish 'skin' treated with EDTA (red line); treated with HCl (green line); untreated (light blue line); and UR-CP-0001 infilling matrix (brown line). (B) Skin sample from *Oreochromis* sp. (Mojarra fish) used for the FTIR analysis and close-up of the skin sample analyzed from this specimen (C). (D) The region from which the 'skin' sample of UR-CP-0001 was taken, and a close-up of the 'skin' fragment after EDTA treatment under a transmitted light microscope (E). (F) UR-CP-0001 sample used for the untreated analysis and a close-up of the FTIR vibrational bands (red rectangle) in (A) after deconvolution (G). (H) UR-CP-0001 infilling matrix sample and how it was grinded using a sterilized mortar and pestle (I) and placed in the FTIR machine (J).

Full-size DOI: [10.7717/peerj.9479/fig-5](https://doi.org/10.7717/peerj.9479/fig-5)

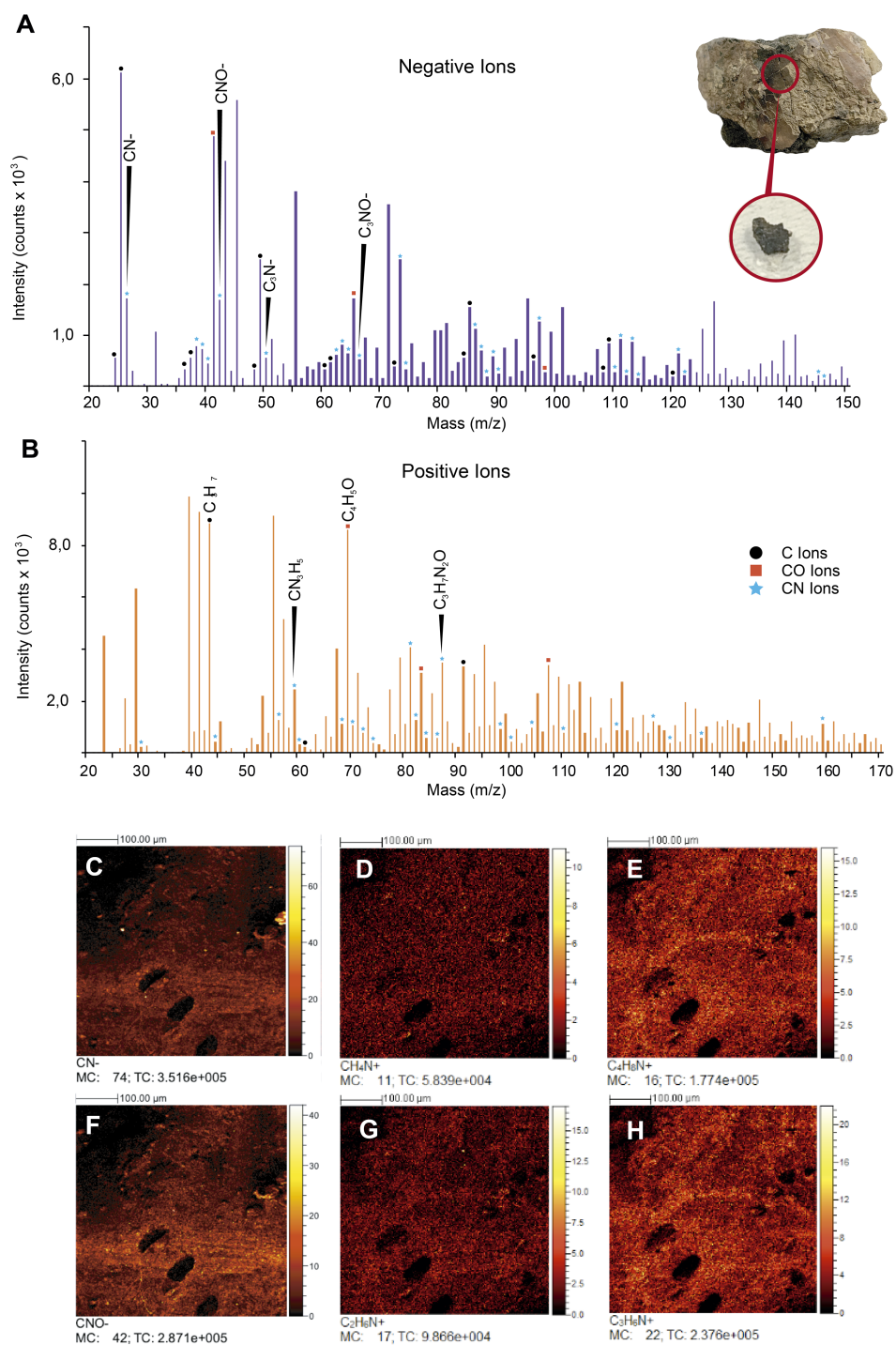


**Figure 6** ToF-SIMS analyses of UR-CP-0001 'skin'. (A–B) Negative and Positive ion ToF-SIMS spectrum of UR-CP-0001 untreated sample (see circular photo of the sample), typical organic compounds occur in high intensities in both ions (raw data presented in [Data S1](#)). (C–H) ToF-SIMS images showing the distribution of ions CN<sup>-</sup>(C), CH<sub>4</sub>N<sup>+</sup>(D), C<sub>4</sub>H<sub>8</sub>N<sup>+</sup>(E), CNO<sup>-</sup>(F), C<sub>2</sub>H<sub>6</sub>N<sup>+</sup>(G) and C<sub>3</sub>H<sub>6</sub>N<sup>+</sup>(H).

Full-size [DOI: 10.7717/peerj.9479/fig-6](https://doi.org/10.7717/peerj.9479/fig-6)

**Table 1** Species tentative assignments and m/z values for peaks in both positive and negative ToF-SIMS spectra from UR-CP-0001 and its possible organic source based on *Samuel et al. (2001)*, *Brüning et al. (2006)*, *Lindgren et al. (2018)* and *Lindgren et al. (2012)*.

Tentative assignment	Theoretical mass	Fossil sample (UR-CP-0001)	Associated organic compound
CN-	26.00	25.997	Melanin
CH <sub>4</sub> N	30.036	29.998	Glycine
CNO-	42.00	42.001	Melanin
C <sub>3</sub> H <sub>7</sub>	43.03	42.998	Leucine
C <sub>2</sub> H <sub>6</sub> N	44.053	43.999	Alanine
C <sub>3</sub> N-	50.00	50.000	Melanin
C <sub>3</sub> H <sub>6</sub> N	56.05	55.996	Lysine
CN <sub>3</sub> H <sub>5</sub>	59.05	59.001	Arginine
C <sub>2</sub> H <sub>6</sub> NO	60.045	59.999	Serine
C <sub>2</sub> H <sub>5</sub> S	61.01	60.998	Methionine
C <sub>3</sub> NO-	66.00	65.996	Melanin
C <sub>4</sub> H <sub>6</sub> N	68.05	67.996	Proline
C <sub>4</sub> H <sub>5</sub> O	69.03	68.998	Threonine
C <sub>4</sub> H <sub>8</sub> N/C <sub>3</sub> H <sub>4</sub> NO	70.068	70.000	Proline
C <sub>4</sub> H <sub>10</sub> N	72.084	71.997	Valine
C <sub>3</sub> H <sub>8</sub> NO	74.063	73.998	Threonine
C <sub>5</sub> N-/C <sub>2</sub> H <sub>2</sub> O <sub>3</sub>	74.00	74.000	Melanin
C <sub>4</sub> H <sub>5</sub> N <sub>2</sub>	81.04	80.996	Histidine
C <sub>4</sub> H <sub>6</sub> N <sub>2</sub>	82.05	81.998	Histidine
C <sub>5</sub> H <sub>7</sub> O	83.09	83.000	Valine
C <sub>5</sub> H <sub>10</sub> N	84.085	84.003	Lysine
C <sub>5</sub> H <sub>12</sub> N/C <sub>4</sub> H <sub>8</sub> NO	86,064/86,101	86.002	Hydroxyproline/Leucine
C <sub>3</sub> H <sub>7</sub> N <sub>2</sub> O	87.05	86.999	Asparagine
C <sub>7</sub> H <sub>7</sub>	91.05	90.998	Phenylalanine
C <sub>4</sub> H <sub>4</sub> NO <sub>2</sub>	98.02	97.999	Asparagine
C <sub>4</sub> H <sub>10</sub> N <sub>3</sub>	100.088	99.999	Arginine
C <sub>4</sub> H <sub>10</sub> NS	104.05	104.002	Methionine
C <sub>7</sub> H <sub>7</sub> O	107.048	106.999	Tyrosine
C <sub>8</sub> N/C <sub>9</sub> H <sub>2</sub>	110.075	109.999	Histidine
C <sub>8</sub> H <sub>10</sub> N	120.084	120.000	Phenylalanine
C <sub>5</sub> H <sub>11</sub> N <sub>4</sub>	127.1	126.997	Arginine
C <sub>9</sub> H <sub>8</sub> N	130.068	130.003	Tryptophan
C <sub>8</sub> H <sub>10</sub> NO	136.082	136.005	Tyrosine
C <sub>10</sub> H <sub>11</sub> N <sub>2</sub>	159.04	159.00	Tryptophan

the organic composition of this layer is its morphological change after being exposed to 10 kV for mapping EDS analysis becoming highly corrugated (Figs. 4E, 4F), which typically happens to uncoated organic tissue or structures under high voltage in SEM similar as degradation of non-conductive materials (*Kersten, 2009*).

FTIR analysis confirmed that the carbon rich layer we found with the EDS is composed of, organic residues, particularly the C-H stretch and  $\nu(\text{C}=\text{O})$  peaks around 2,931 and

1,737 respectively (Fig. 5A), which are commonly found in collagen I (Belbachir *et al.*, 2009; Jeevithan *et al.*, 2014; Valenzuela-Rojo, López-Cervantes & Sánchez-Machado, 2018) and keratin (Chandini *et al.*, 2017; Estévez-Martínez *et al.*, 2013); highly abundant proteins found in the scales and skin of fishes (Bhagwat & Dandge, 2016; Elliott, 2011). Amide A, I, II, and III, C-H stretch and  $\nu(\text{C}=\text{O})$  peaks were clearly observed in the FTIR of the extant *Oreochromis* sp. (mojarra fish) skin used as standard for comparison (Fig. 5A). Peaks potentially corresponding to Amide I and II were also found in the deconvoluted spectrum of the 'skin' untreated sample (Fig. 5D), falling inside the range of vibrational bands as product of possible diagenetic alterations of the original organic compounds, similar as occurs in FTIR analyses of modern proteins (Kong & Yu, 2007). We exclude a potential bacterial origin of the organic component of the 'skin' in UR-CP-0001 because FTIR spectra lack of the characteristic broad infrared absorption band of hydroxyl group (-OH) of polysaccharides at  $3,700\text{--}3,100\text{ cm}^{-1}$  (Lee *et al.*, 2017; Lindgren *et al.*, 2011b). ToF-SIMS results of the two samples of UR-CP-0001 analyzed also show the occurrence of molecular organic fragments, including the positive  $\text{CH}_4\text{N}^+$  (Fig. 6D),  $\text{C}_4\text{H}_8\text{N}^+$  (Fig. 6E),  $\text{C}_2\text{H}_6\text{N}^+$  (Fig. 6G),  $\text{C}_3\text{H}_6\text{N}^+$  (Fig. 6H) and  $\text{C}_7\text{H}_7\text{O}^+$  which are typical residues of glycine, alanine, proline and tyrosine constituents of collagen and fibronectin (Brüning *et al.*, 2006; Hens *et al.*, 2013). Two other ions that support potential organic preservation in the 'skin' of UR-CP-0001 are  $\text{CN}^-$  (Fig. 6C) and  $\text{CNO}^-$  (Fig. 6F) negative ions particularly abundant in melanosomes and melanin (Lindgren *et al.*, 2018; Lindgren *et al.*, 2012), and although we can not reject at this point that they could be from another source, our hypothesis seems to be plausible. A complete tentative assignment of ions derived from proteins based on  $m/z$  values in UR-CP-0001 samples and theoretical mass is presented in Table 1. We exclude a potential mineralized biofilm source of protein residues based on the FTIR spectra (Fig. 5A) and the absence of any morphological features associated to bacteria origin (filaments or spheres) (Kaye, Gaugler & Sawlowicz, 2008; Schweitzer, Moyer & Zheng, 2016).

The preservation of the 'skin' in UR-CP-001 is also supported by its morphological corrugated macroscopic appearance (Figs. 2G, 3E) resembling a phenomenon that occurs to the skin from extant fishes where an absence of scales leaves the skin without an external support structure, make it more susceptible to wrinkling under a compression stress (Vernerey & Barthelat, 2014), due to dehydration or in a post mortem deformation (Lindgren *et al.*, 2018) (Figs. 3C, 3E). Additionally, collagen fibers were observed in both UR-CP-0001 'skin' and the dehydrated skin from extant *Oreochromis* sp. (mojarra fish) also to microscopic level after EDTA demineralization of 'skin' (Figs. 3D, 3G, 3H) supporting the interpretation of UR-CP-0001 as an exceptional preserved fossilized skin.

## DISCUSSION

Aspidorhynchid fishes had widespread geographic and temporal distribution with fossils reported in all continents from the Middle Jurassic to Late Cretaceous (Brito, 1997). Specimen UR-CP-0001 represents the earliest known record for an aspidorynchid in Colombia, extending the temporal range from the Aptian (Schultze & Stöhr, 1996) to Barremian. Once again, a peri-Gondwanan distribution of *Vinctifer* (Fig. S3) is confirmed here, as UR-CP-0001 potentially belongs to this genus (see Remarks).

Vibrational spectroscopic techniques such FTIR demonstrates its reliability to understand fossil preservation mechanisms, due to its sensitiveness to organic functional groups and phosphates through high peak bands (*Lafuente-Diaz et al., 2020; Olcott Marshall & Marshall, 2015*). However, due to noise signals, a deconvolution was needed to unveil masked absorbance peaks from the raw data. ToF-SIMS also give more resolution to identify the nature of preserved components. These kind of analysis has demonstrate to be trustful for inferences about preservation mechanisms and track the origin of the preserved molecules (*Bezerra et al., 2020; Lafuente-Diaz et al., 2020*).

Although it is hard to reconstruct the complete chain of taphonomical events that occurred to UR-CP-0001, we hypothesize that besides fragmentation and fins disarticulation without losing the conical shape of its caudal region, the nature of its scales and skin played a key role in its preservation. The presence of scales and the thickness of the fossilized 'skin' suggest a possible mechanism of preservation that we call a "microsandwich effect", which could apply to many other fragmentary fossil fishes that have not been studied for molecular paleontology. Scales may have acted as an external barrier against bacteria and other environmental decay accelerators, which could decompose the integument. Simultaneously, the basal layer became enriched in phosphate, possibly resulting from the degradation of phosphate containing organic compounds from the dermis itself, as has been reported in other fossilized skin from vertebrates (*McNamara et al., 2009*), at the same time this layer may have acted as an internal barrier, creating an encapsulating environment for the integument. These local biogeochemical interactions would favor not only preservation of the general morphology of the skin, but also some of their soft-tissue structures and residues of the original biomolecules by geopolymerization (*Lindgren et al., 2018*). Another factor that potentially played a key role in the preservation of the 'skin' in UR-CP-0001 was the burial environment conditions, dominated by organic-rich shale interval showing characteristics of oxygen depleted conditions at the lower segment of Paja Formation in this region (*Gaona-Narvaez, Florentin & Etayo-Serna, 2013*). Microcrystalline minerals like clays and shales have extremely large surface area to volume ratios, and are usually charged, both of which favor adsorption and inactivation of degrading enzymes, similar been proposed for the exceptional preservation of Burgess Shale fossils (*Butterfield, 1990*).

Our results imply that the Paja Formation could be potentially considered as the third locality in South America where exceptional preservation in fishes have been reported, alongside of the Brazilian Romualdo and Crato Formations, where the preservation mechanisms is well known (*Osés et al., 2017*). The mechanism of preservation proposed here, as well as other recent work (*Lindgren et al., 2018*) increases the number of potential scenarios for preservation of cellular-to-subcellular soft tissue morphology in fossils additional to oxidative depositional environments (*Wiemann et al., 2018*), where iron play a key role (*Schweitzer et al., 2014*). As we showed in here, iron was not detected in UR-CP-0001, suggesting that in molecular paleontology studies there will be always exceptions to those formulated general trends and factors favoring preservation in deep time, and that each case and fossil site needs to be considered with its own particularities.

## CONCLUSIONS

Exceptional preserved 'skin' from an aspidorhynchid fish represents the first report of soft tissue preservation in vertebrates from the Early Cretaceous in north South America. Morphological comparisons and molecular analyses present several similar features between the extant fish skin and the fossilized specimen. Molecular analyses also provide evidence of possible proteinaceous residues preserved in the fossilized skin, which is supported by vibrational peaks associated with Amide I and II in the FTIR spectra and signals that can be associated to aminoacids like Glycine and Lysine. Because of the limitation in the project funding, future analyses should be focused on immunohistochemistry, testing specific fish skin antibodies and other mass spectrometry techniques including LC-MS/MS to confirm the preservation of original proteinaceous components.

### Institutional abbreviation

**UR-CP** paleontological collection, Facultad de Ciencias Naturales y Matemáticas, Universidad del Rosario, Bogotá, Colombia.

## ACKNOWLEDGEMENTS

We thank to E Realpe for allowing us to use the stereomicroscope. Special thanks to A Link for helping us with the logistics. Thanks to M Negrete and the radiology team at the Hospital Méderi for access to the CT-scan. Thanks to M López and H Pinto from the Universidad de los Andes, Bogotá for the scanning this fossil with the SEM-EDS and the analyses performed with the FTIR spectrometer. Thanks to Y Rojas for allow us the use of the polarized transmitted light microscope at Universidad de los Andes. Thanks to A Forero and L Daza for assistance during lab preparation of the samples. Thanks to C Zhou for the ToF-SIMS analyses. Special thanks to M Schweitzer and JA Wilson, as well as to M. Benton and an anonymous reviewer for valuable comments on the manuscript.

## ADDITIONAL INFORMATION AND DECLARATIONS

### Funding

Funding for this project was granted to Edwin Alberto Cadena from Universidad del Rosario, Capital Semilla grants program 2019 and Fondos de Arranque 2018: (Code IV-TFA022). The funders had no role in study design, data collection and analysis, decision to publish, or preparation of the manuscript.

### Grant Disclosures

The following grant information was disclosed by the authors:

Edwin Alberto Cadena from Universidad del Rosario, Capital Semilla grants program 2019. Fondos de Arranque 2018: (Code IV-TFA022).

### Competing Interests

The authors declare there are no competing interests.



## Author Contributions

- Andrés Alfonso-Rojas conceived and designed the experiments, performed the experiments, analyzed the data, prepared figures and/or tables, authored or reviewed drafts of the paper, photos, and approved the final draft.
- Edwin-Alberto Cadena conceived and designed the experiments, performed the experiments, analyzed the data, prepared figures and/or tables, authored or reviewed drafts of the paper, fieldwork, and approved the final draft.

## Field Study Permissions

The following information was supplied relating to field study approvals (i.e., approving body and any reference numbers):

Field experiments were approved by the Comité de ética and the Dirección de Investigaciones of the Universidad del Rosario (IV-FCS018).

## Data Availability

The following information was supplied regarding data availability:

Raw data is available in the [Supplementary Files](#).

## Supplemental Information

Supplemental information for this article can be found online at <http://dx.doi.org/10.7717/peerj.9479#supplemental-information>.

## REFERENCES

- Bailleul AM, Zheng W, Horner JR, Hall BK, Holliday CM, Schweitzer MH. 2020. Evidence of proteins, chromosomes and chemical markers of DNA in exceptionally preserved dinosaur cartilage. *National Science Review* 0:1–8.
- Belbachir K, Noreen R, Gousspillou G, Petibois C. 2009. Collagen types analysis and differentiation by FTIR spectroscopy. *Analytical and Bioanalytical Chemistry* 395:829–837 DOI 10.1007/s00216-009-3019-y.
- Bezerra FI, Da Silva JH, De Castro Miguel E, Paschoal AR, Nascimento DR, Freire PT, Viana BC, Mendes M. 2020. Chemical and mineral comparison of fossil insect cuticles from Crato Konservat Lagerstätte, Lower Cretaceous of Brazil. *Journal of Iberian Geology* 46:61–76.
- Bhagwat PK, Dandge PB. 2016. Isolation, characterization and valorizable applications of fish scale collagen in food and agriculture industries. *Biocatalysis and Agricultural Biotechnology* 7:234–240 DOI 10.1016/j.bcab.2016.06.010.
- Boatman E, Goodwin MB, Holman HYN, Fakra SC, Zheng W, Gronsky R, Schweitzer MH. 2019. Mechanisms of soft tissue and protein preservation in *Tyrannosaurus rex*. *Scientific Reports* 9:15678 DOI 10.1038/s41598-019-51680-1.
- Bosch-Reig FB, Gimeno-Adelantado JVG, Moya-Moreno MCM. 2002. FTIR quantitative analysis of calcium carbonate (calcite) and silica (quartz) mixtures using the constant ratio method. Applications to geological samples. *Talanta* 58:811–821 DOI 10.1016/S0039-9140(02)00372-7.

- Brito PM. 1997.** Révision des Aspidorhynchidae (Pisces, Actinopterygii) du Mésozoïque: ostéologie, relations phylogénétiques, données environnementales et biogéographiques. *Geodiversitas* **19**:681–772.
- Brown CM, Henderson DM, Vinther J, Fletcher I, Sistiaga A, Herrera J, Summons RE. 2017.** An exceptionally preserved three-dimensional armored dinosaur reveals insights into coloration and Cretaceous predator–prey dynamics. *Current Biology* **27**:2514–2521 DOI [10.1016/j.cub.2017.06.071](https://doi.org/10.1016/j.cub.2017.06.071).
- Brüning C, Hellweg S, Dambach S, Lipinsky D, Arlinghaus HF. 2006.** Improving the interpretation of ToF-SIMS measurements on adsorbed proteins using PCA. *Surface and Interface Analysis* **38**:191–193 DOI [10.1002/sia.2233](https://doi.org/10.1002/sia.2233).
- Butterfield NJ. 1990.** Organic preservation of non-mineralizing organisms and the taphonomy of the Burgess Shale. *Paleobiology* **16**:272–286 DOI [10.1017/S0094837300009994](https://doi.org/10.1017/S0094837300009994).
- Cadena EA. 2015.** The first South American sandownid turtle from the Lower Cretaceous of Colombia. *PeerJ* **3**:e1431 DOI [10.7717/peerj.1431](https://doi.org/10.7717/peerj.1431).
- Cadena E. 2016.** Microscopical and elemental FESEM and Phenom ProX-SEM-EDS analysis of osteocyte-and blood vessel-like microstructures obtained from fossil vertebrates of the Eocene Messel Pit, Germany. *PeerJ* **4**:e1618 DOI [10.7717/peerj.1618](https://doi.org/10.7717/peerj.1618).
- Cadena EA, Parham JF. 2015.** Oldest known marine turtle? A new protostegid from the Lower Cretaceous of Colombia. *PaleoBios* **32**:1–45.
- Cadena EA, Parra-Ruge ML, Parra-Ruge JdD, Padilla-Bernal S. 2019.** A gravid fossil turtle from the Early Cretaceous reveals a different egg development strategy to that of extant marine turtles. *Palaeontology* **62**:533–545 DOI [10.1111/pala.12413](https://doi.org/10.1111/pala.12413).
- Cadena EA, Schweitzer MH. 2012.** Variation in osteocytes morphology vs. bone type in turtle shell and their exceptional preservation from the Jurassic to the present. *Bone* **51**:614–620 DOI [10.1016/j.bone.2012.05.002](https://doi.org/10.1016/j.bone.2012.05.002).
- Caldwell MW, Sasso CD. 2004.** Soft-tissue preservation in a 95 million year old marine lizard: form, function, and aquatic adaptation. *Journal of Vertebrate Paleontology* **24**:980–985 DOI [10.1671/0272-4634\(2004\)024\[0980:SPIAMY\]2.0.CO;2](https://doi.org/10.1671/0272-4634(2004)024[0980:SPIAMY]2.0.CO;2).
- Cantalice KM, Alvarado-Ortega J, Brito PM. 2018.** Sobre la ocurrencia de *Vinctifer ferusquiai* sp. nov. (Actinopterygii, Aspidorhynchiformes) en los depósitos Kimmeridgianos (Jurásico Tardío) cercanos a Tlaxiaco, Oaxaca, sur de México. *Revista Mexicana de Ciencias Geológicas* **35**:179–187 DOI [10.22201/cgeo.20072902e.2018.2.713](https://doi.org/10.22201/cgeo.20072902e.2018.2.713).
- Carballido JL, Pol D, Parra-Ruge ML, Padilla-Bernal S, Páramo-Fonseca ME, Etayo-Serna F. 2015.** A new Early Cretaceous brachiosaurid (Dinosauria, Neosauropoda) from northwestern Gondwana (Villa de Leiva, Colombia). *Journal of Vertebrate Paleontology* **35**:1–12 DOI [10.1080/02724634.2015.1127721](https://doi.org/10.1080/02724634.2015.1127721).
- Chandini DS, Charulatha M, Legadevi R, Meignanalakshmi S. 2017.** In vitro evaluation of natural keratin based hydrogel from chicken feather waste for controlled drug release. *International Journal of Current Microbiology Applied Science* **6**:3488–3495.
- Chernova O. 2009.** Skin derivatives in vertebrate ontogeny and phylogeny. *Biology Bulletin* **36**:175–183 DOI [10.1134/S1062359009020101](https://doi.org/10.1134/S1062359009020101).

- Cleland TP, Schroeter ER, Zamdborg L, Zheng W, Lee JE, Tran JC, Bern M, Duncan MB, Lebleu VS, Ahlf DR. 2015.** Mass spectrometry and antibody-based characterization of blood vessels from *Brachylophosaurus canadensis*. *Journal of Proteome Research* **14**:5252–5262 DOI [10.1021/acs.jproteome.5b00675](https://doi.org/10.1021/acs.jproteome.5b00675).
- Coria RA, Chiappe LM. 2007.** Embryonic skin from Late Cretaceous sauropods (Dinosauria) of Auca Mahuevo, Patagonia, Argentina. *Journal of Paleontology* **81**:1528–1532 DOI [10.1666/05-150.1](https://doi.org/10.1666/05-150.1).
- Elliott D. 2011.** Functional morphology of the integumentary system in fishes. In: Farrell AP, ed. *Encyclopedia of fish physiology: from genome to environment*. Vol. 1. San Diego: Academic Press, 476–488.
- Estévez-Martínez Y, Velasco-Santos C, Martínez-Hernández A-L, Delgado G, Cuevas-Yáñez E, Alaníz-Lumbreras D, Duron-Torres S, Castaño VM. 2013.** Grafting of multiwalled carbon nanotubes with chicken feather keratin. *Journal of Nanomaterials* **2013**:702157.
- Gaona-Narvaez T, Florentin J-MM, Etayo-Serna F. 2013.** Geochemistry, palaeoenvironments and timing of Aptian organic-rich beds of the Paja Formation (Curití, Eastern Cordillera, Colombia). *Geological Society, London, Special Publications* **382**:31–48 DOI [10.1144/SP382.6](https://doi.org/10.1144/SP382.6).
- Grellet-Tinner G, Codrea V, Folie A, Higa A, Smith T. 2012.** First evidence of reproductive adaptation to Island effect of a dwarf Cretaceous Romanian titanosaur, with embryonic integument in ovo. *PLOS ONE* **7**:e32051 DOI [10.1371/journal.pone.0032051](https://doi.org/10.1371/journal.pone.0032051).
- Hall JP, Wolberg DL, West S. 1988.** Dinosaur-skin impressions from the Fruitland Formation (Campanian–Maastrichtian) of the Fossil Forest, San Juan Basin, San Juan County, New Mexico. *New Mexico Bureau of Mines and Mineral Resources Bulletin* **122**:23–27.
- Henss A, Rohnke M, El Khassawna T, Govindarajan P, Schlewitz G, Heiss C, Janek J. 2013.** Applicability of ToF-SIMS for monitoring compositional changes in bone in a long-term animal model. *Journal of The Royal Society Interface* **10**:20130332 DOI [10.1098/rsif.2013.0332](https://doi.org/10.1098/rsif.2013.0332).
- Jeevithan E, Bao B, Bu Y, Zhou Y, Zhao Q, Wu W. 2014.** Type II collagen and gelatin from silvertip shark (*Carcharhinus albimarginatus*) cartilage: isolation, purification, physicochemical and antioxidant properties. *Marine Drugs* **12**:3852–3873 DOI [10.3390/md12073852](https://doi.org/10.3390/md12073852).
- Kaye TG, Gaugler G, Sawlowicz Z. 2008.** Dinosaurian soft tissues interpreted as bacterial biofilms. *PLOS ONE* **3**:e2808 DOI [10.1371/journal.pone.0002808](https://doi.org/10.1371/journal.pone.0002808).
- Kellner AW, Campos DA, Sayao JM, Saraiva AA, Rodrigues T, Oliveira G, Cruz LA, Costa FR, Silva HP, Ferreira JS. 2013.** The largest flying reptile from Gondwana: a new specimen of *Tropeognathus* cf. *T. mesembrinus* Wellnhofer, 1987 (Pterodactyloidea, Anhangueridae) and other large pterosaurs from the Romualdo Formation, Lower Cretaceous, Brazil. *Anais da Academia Brasileira de Ciências* **85**:113–135 DOI [10.1590/S0001-37652013000100009](https://doi.org/10.1590/S0001-37652013000100009).

- Kersten K. 2009.** Sample degradation during SEM analysis: what causes it and how to slow down the process. Available at <https://blog.phenom-world.com/> (accessed on February 2020).
- Kong J, Yu S. 2007.** Fourier transform infrared spectroscopic analysis of protein secondary structures. *Acta Biochimica et Biophysica Sinica* **39**:549–559 DOI [10.1111/j.1745-7270.2007.00320.x](https://doi.org/10.1111/j.1745-7270.2007.00320.x).
- Lafuente-Diaz MA, D'Angelo JA, Del Fueyo GM, Carrizo MA. 2020.** FTIR spectroscopic features of the pteridosperm *Rufflorinia orlandoi* and host rock (Springhill Formation, Lower Cretaceous, Argentina). *Journal of South American Earth Sciences* **99**:102520 DOI [10.1016/j.jsames.2020.102520](https://doi.org/10.1016/j.jsames.2020.102520).
- Lee Y-C, Chiang C-C, Huang P-Y, Chung C-Y, Huang TD, Wang C-C, Chen C-I, Chang R-S, Liao C-H, Reisz RR. 2017.** Evidence of preserved collagen in an Early Jurassic sauropodomorph dinosaur revealed by synchrotron FTIR microspectroscopy. *Nature Communications* **8**:14220 DOI [10.1038/ncomms14220](https://doi.org/10.1038/ncomms14220).
- Lindgren J, Everhart MJ, Caldwell MW. 2011a.** Three-dimensionally preserved integument reveals hydrodynamic adaptations in the extinct marine lizard *Ectenosaurus* (Reptilia, Mosasauridae). *PLOS ONE* **6**:e27343 DOI [10.1371/journal.pone.0027343](https://doi.org/10.1371/journal.pone.0027343).
- Lindgren J, Kaddumi HF, Polcyn MJ. 2013.** Soft tissue preservation in a fossil marine lizard with a bilobed tail fin. *Nature Communications* **4**:2423 DOI [10.1038/ncomms3423](https://doi.org/10.1038/ncomms3423).
- Lindgren J, Sjövall P, Thiel V, Zheng W, Ito S, Wakamatsu K, Hauff R, Kear BP, Engdahl A, Alwmark C. 2018.** Soft-tissue evidence for homeothermy and crypsis in a Jurassic ichthyosaur. *Nature* **564**:359–365 DOI [10.1038/s41586-018-0775-x](https://doi.org/10.1038/s41586-018-0775-x).
- Lindgren J, Uvdal P, Engdahl A, Lee AH, Alwmark C, Bergquist KE, Nilsson E, Ekström P, Rasmussen M, Douglas DA, Polcyn MJ, Jacobs LL. 2011b.** Microspectroscopic evidence of Cretaceous bone proteins. *PLOS ONE* **6**:e19445 DOI [10.1371/journal.pone.0019445](https://doi.org/10.1371/journal.pone.0019445).
- Lindgren J, Uvdal P, Sjövall P, Nilsson E, Engdahl A, Schultz BP, Thiel V. 2012.** Molecular preservation of the pigment melanin in fossil melanosomes. *Nature Communications* **3**:824 DOI [10.1038/ncomms1819](https://doi.org/10.1038/ncomms1819).
- Lingham-Soliar T, Plodowski G. 2010.** The integument of *Psittacosaurus* from Liaoning Province, China: taphonomy, epidermal patterns and color of a ceratopsian dinosaur. *Naturwissenschaften* **97**:479–486 DOI [10.1007/s00114-010-0661-3](https://doi.org/10.1007/s00114-010-0661-3).
- Maisey JG. 1991.** *Santana fossils: an illustrated atlas*. Neptune City: TFH Publications Incorporated, Neptune, 462.
- Manning PL, Morris PM, McMahon A, Jones E, Gize A, Macquaker JH, Wolff G, Thompson A, Marshall J, Taylor KG. 2009.** Mineralized soft-tissue structure and chemistry in a mummified hadrosaur from the Hell Creek Formation, North Dakota (USA). *Proceedings of the Royal Society B: Biological Sciences* **276**:3429–3437 DOI [10.1098/rspb.2009.0812](https://doi.org/10.1098/rspb.2009.0812).
- Martill DM. 1988.** Preservation of fish in the Cretaceous Santana Formation Brazil. *Palaeontology* **31**:1–18.

- Martill DM. 1989.** The Medusa effect: instantaneous fossilization. *Geology Today* 5:201–205 DOI [10.1111/j.1365-2451.1989.tb00671.x](https://doi.org/10.1111/j.1365-2451.1989.tb00671.x).
- Martin T, Marugán-Lobón J, Vullo R, Martín-Abad H, Luo Z-X, Buscalioni AD. 2015.** A Cretaceous eutriconodont and integument evolution in early mammals. *Nature* 526:380–384 DOI [10.1038/nature14905](https://doi.org/10.1038/nature14905).
- Maxwell EE, Cortés D, Patarroyo P, Ruge MLP. 2019.** A new specimen of *Platypterygius sachicarum* (Reptilia, Ichthyosauria) from the Early Cretaceous of Colombia and its phylogenetic implications. *Journal of Vertebrate Paleontology* 39:e1577875 DOI [10.1080/02724634.2019.1577875](https://doi.org/10.1080/02724634.2019.1577875).
- McNamara ME, Kaye JS, Benton MJ, Orr PJ, Rossi V, Ito S, Wakamatsu K. 2018b.** Non-integumentary melanosomes can bias reconstructions of the colours of fossil vertebrates. *Nature Communications* 9:2878 DOI [10.1038/s41467-018-05148-x](https://doi.org/10.1038/s41467-018-05148-x).
- McNamara ME, Orr PJ, Kearns SL, Alcalá L, Anadón P, Peñalver Mollá E. 2009.** Soft-tissue preservation in Miocene frogs from Libros, Spain: insights into the genesis of decay microenvironments. *Palaios* 24:104–117 DOI [10.2110/palo.2008.p08-017r](https://doi.org/10.2110/palo.2008.p08-017r).
- McNamara ME, Orr PJ, Kearns SL, Alcalá L, Anadón P, Peñalver E. 2016.** Reconstructing carotenoid-based and structural coloration in fossil skin. *Current Biology* 26:1075–1082 DOI [10.1016/j.cub.2016.02.038](https://doi.org/10.1016/j.cub.2016.02.038).
- McNamara ME, Zhang F, Kearns SL, Orr PJ, Toulouse A, Foley T, Hone DW, Rogers CS, Benton MJ, Johnson D. 2018a.** Fossilized skin reveals coevolution with feathers and metabolism in feathered dinosaurs and early birds. *Nature Communications* 9:2072 DOI [10.1038/s41467-018-04443-x](https://doi.org/10.1038/s41467-018-04443-x).
- Micklich N. 2002.** The fish fauna of Messel Pit: a nursery school? *Courier-Forschungsinstitut Senckenberg* 237:97–127.
- Noé LF, Gómez-Pérez M. 2020.** Plesiosaurs, palaeoenvironments, and the Paja Formation Lagerstätte of central Colombia: an overview. In: Gómez J, Pinilla-Pachon AO, eds. *The Geology of Colombia, Volume 2 Mesozoic. Servicio Geológico Colombiano, Publicaciones Geológicas Especiales* 36, 43 p. Bogotá DOI [10.32685/pub.esp.36.2019.13](https://doi.org/10.32685/pub.esp.36.2019.13).
- Olcott Marshall A, Marshall CP. 2015.** Vibrational spectroscopy of fossils. *Palaeontology* 58:201–211 DOI [10.1111/pala.12144](https://doi.org/10.1111/pala.12144).
- Osés GL, Petri S, Voltani CG, Prado GM, Galante D, Rizzutto MA, Rudnitzki ID, Da Silva EP, Rodrigues F, Rangel EC. 2017.** Deciphering pyritization-kerogenization gradient for fish soft-tissue preservation. *Scientific Reports* 7:1–15 DOI [10.1038/s41598-016-0028-x](https://doi.org/10.1038/s41598-016-0028-x).
- Paik IS, Kim HJ, Huh M. 2010.** Impressions of dinosaur skin from the Cretaceous Haman Formation in Korea. *Journal of Asian Earth Sciences* 39:270–274 DOI [10.1016/j.jseaes.2010.02.015](https://doi.org/10.1016/j.jseaes.2010.02.015).
- Páramo-Fonseca ME, Gómez-Pérez M, Noé LF, Etayo-Serna F. 2016.** *Stenorhynchosaurus munozi*, gen. et sp. nov. a new pliosaurid from the Upper Barremian (Lower Cretaceous) of Villa de Leiva, Colombia, South America. *Revista de la Academia Colombiana de Ciencias Exactas, Físicas, y Naturales* 40:84–103 DOI [10.18257/racefyn.239](https://doi.org/10.18257/racefyn.239).

- Patarroyo P. 2009.** Amonitas de un nivel de alta energía del Barremiano inferior en la Formación Paja de los sectores de Villa de Leyva (Boyacá) y de Vélez (Santander). *Boletín de Geología* 31:15–21.
- Patarroyo P. 2020.** Barremian deposits of Colombia: a special emphasis on marine successions. In: Gómez J, Pinilla-Pachon AO, eds. *The Geology of Colombia, Volume 2 Mesozoic. Servicio Geológico Colombiano, Publicaciones Geológicas Especiales* 36, 37 p. Bogotá DOI 10.32685/pub.esp.36.2019.12.
- Samuel NT, Wagner MS, Dornfeld KD, Castern DG. 2001.** Analysis of poly (amino acids) by static time-of-flight secondary ion mass spectrometry (TOF-SIMS). *Surface Science Spectra* 8:163–184 DOI 10.1116/11.20020301.
- Schultze H-P, Stöhr D. 1996.** *Vinctifer* (Pisces, Aspidorhynchidae) aus der unterkreide (oberes Aptium) von Kolumbien. *Neues Jahrbuch für Geologie und Paläontologie-Abhandlungen* 199:395–415 DOI 10.1127/njgpa/199/1996/395.
- Schweitzer MH. 2011.** Soft tissue preservation in terrestrial Mesozoic vertebrates. *Annual Review of Earth and Planetary Sciences* 39:187–216 DOI 10.1146/annurev-earth-040610-133502.
- Schweitzer MH, Moyer AE, Zheng W. 2016.** Testing the hypothesis of biofilm as a source for soft tissue and cell-like structures preserved in dinosaur bone. *PLOS ONE* 11:e0150238 DOI 10.1371/journal.pone.0150238.
- Schweitzer MH, Zheng W, Cleland TP, Goodwin MB, Boatman E, Theil E, Marcus MA, Fakra SC. 2014.** A role for iron and oxygen chemistry in preserving soft tissues, cells and molecules from deep time. *Proceedings of the Royal Society B: Biological Sciences* 281:20132741 DOI 10.1098/rspb.2013.2741.
- Signore M, Bucci E, Pede C, Barbera C. 2005.** A new ichthyodectid fish from the Lower Cretaceous of Pietraroja (Southern Italy). *PalArch* 5:25–29.
- Sionkowska A, Kozłowska J. 2014.** Fish scales as a biocomposite of collagen and calcium salts. *Key Engineering Materials* 587:185–190.
- Sousa Filho F, Da Silva J, Saraiva G, Abagaro B, Barros O, Saraiva A, Viana B, Freire P. 2016.** Spectroscopic studies of the fish fossils (*Cladocyclus gardneri* and *Vinctifer comptoni*) from the Ipubi Formation of the Cretaceous Period. *Spectrochimica Acta Part A: Molecular and Biomolecular Spectroscopy* 157:124–128 DOI 10.1016/j.saa.2015.12.022.
- Valenzuela-Rojo DR, López-Cervantes J, Sánchez-Machado DI. 2018.** Tilapia (*Oreochromis aureus*) Collagen for Medical Biomaterials. *Seaweed Biomaterials* 6:47–66 DOI 10.5772/intechopen.77051.
- Varejão FG, Warren LV, Simões MG, Fürsich FT, Matos SA, Assine ML. 2019.** Exceptional preservation of soft tissues by microbial entombment: insights into the taphonomy of the Crato Konservat-Lagerstätte. *Palaios* 34:331–348 DOI 10.2110/palo.2019.041.
- Vernerey FJ, Barthelat F. 2014.** Skin and scales of teleost fish: simple structure but high performance and multiple functions. *Journal of the Mechanics and Physics of Solids* 68:66–76 DOI 10.1016/j.jmps.2014.01.005.

- Vernygora O, Murray AM, Luque J, Ruge MLP, Fonseca MEP. 2018.** A new Cretaceous dercetid fish (Neoteleostei: Aulopiformes) from the Turonian of Colombia. *Journal of Systematic Palaeontology* **16**:1057–1071 DOI [10.1080/14772019.2017.1391884](https://doi.org/10.1080/14772019.2017.1391884).
- Wiemann J, Fabbri M, Yang T-R, Stein K, Sander PM, Norell MA, Briggs DE. 2018.** Fossilization transforms vertebrate hard tissue proteins into N-heterocyclic polymers. *Nature Communications* **9**:4741 DOI [10.1038/s41467-018-07013-3](https://doi.org/10.1038/s41467-018-07013-3).
- Xu X, Zhou Z, Wang Y, Wang M. 2020.** Study on the Jehol Biota: recent advances and future prospects. *Science China Earth Sciences* **63**:757–773.